PHYSICAL REVIEW B **95**, 235156 (2017)

Magnetism and charge density waves in $RNiC_2$ (R = Ce, Pr, Nd)

Kamil K. Kolincio,* Marta Roman, Michał J. Winiarski, Judyta Strychalska-Nowak, and Tomasz Klimczuk†
Faculty of Applied Physics and Mathematics, Gdansk University of Technology, Narutowicza 11/12, 80-233 Gdansk, Poland
(Received 14 April 2017; published 29 June 2017)

We have compared the magnetic, transport, galvanomagnetic, and specific-heat properties of $CeNiC_2$, $PrNiC_2$, and $NdNiC_2$ to study the interplay between charge density waves (CDW) and magnetism in these compounds. The negative magnetoresistance in $NdNiC_2$ is discussed in terms of the partial destruction of charge density waves and an irreversible phase transition stabilized by the field-induced ferromagnetic transformation is reported. For $PrNiC_2$ we demonstrate that the magnetic field initially weakens the CDW state, due to the Zeeman splitting of conduction bands. However, the Fermi surface nesting is enhanced at a temperature related to the magnetic anomaly.

DOI: 10.1103/PhysRevB.95.235156

I. INTRODUCTION

The interaction between charge density waves (CDW) and different types of orderings such as superconductivity [1–3], spin density waves [4–6], and magnetism [7] has been a long-standing area of interest. Magnetic order or applied magnetic field have been found to impact the CDW state through changing the geometry of the Fermi surface (FS). The effect can be destructive due to the disturbance of the FS nesting caused by the magnetic field-induced splitting of the conduction bands or modification of the electronic structure due to a magnetic transition [8]. Alternatively, a constructive effect has been observed in a group of materials, in which this FS transformation leads to the enhancement of the nesting conditions or when the nesting vector has the ability to adapt to the evolution of the Fermi surface [9–15]. Recently, much attention of the researchers exploring the coupling between CDW, superconductivity, and magnetic order has been devoted to the two families of ternary compounds: $M_5Ir_4Si_{10}$ (where M = Y, Dy, Ho, Er, Tm, Yb, or Lu) [16–24] and $RNiC_2$ (where R = La, Ce, Pr, Nd, Sm, Gd, or Tb) [25,26]. Most of the members of the latter family exhibit the Peierls transitions towards the charge density wave state [27]. The relevance of a Peierls instability has been confirmed for R = Gd, Tb, Nd, Pr, and Sm, while the $LaNiC_2$ and $CeNiC_2$ compounds do not show any anomalies that could be attributed to CDW [28–32]. Instead, $LaNiC_2$ is an unconventional noncentrosymmetric superconductor with T_c = 2.7 K [33–35]. Next to the CDW, the members of the $RNiC_2$ family show a wide range of magnetic orderings originating from the Ruderman-Kittel-Kasuya-Yosida (RKKY) interaction between local magnetic moments and conduction electrons [36,37]. The ground state of $RNiC_2$ depends on the rare-earth atom marked in the above formula by R: $CeNiC_2$, $NdNiC_2$, $GdNiC_2$, and $TbNiC_2$ show the antiferromagnetic (AFM) character [34,38–42], $SmNiC_2$ is a ferromagnet, while the $PrNiC_2$ compound has been identified as a van Vleck paramagnet [43]. This rich variety of the types of magnetic ordering shown by the $RNiC_2$ family members motivated us to explore the interplay of charge density waves and various magnetic ground states. Here, we compare the physical properties of three isostructural, yet highly dissimilar compounds: $NdNiC_2$, $PrNiC_2$, and $CeNiC_2$. The first compound, $NdNiC_2$, shows the Peierls instability with T_P = 121 K and antiferromagnetic ordering with T_N = 17 K. The second, $PrNiC_2$, undergoes the CDW transition at T_P = 89 K and, instead of long-range magnetic ordering, shows a magnetic anomaly at T^* = 8 K. The last compound, $CeNiC_2$, becomes an antiferromagnet at T_N = 20 K and does not exhibit the CDW transition.

II. EXPERIMENTAL DETAILS

The polycrystalline samples of $RNiC_2$ (where R = Ce, Pr, and Nd) were synthesized by arc melting the stoichiometric amounts of pure elements—Ni (4N), C (5N), Ce (3N), Pr (3N), and Nd (3N)—in a high-purity argon atmosphere. Small excess of Ce, Pr, Nd (≈2%), and C (≈5%) was used to compensate the loss during arc melting. To obtain good homogeneity of samples, the specimens were turned over and remelted four times in a water-cooled copper hearth. A zirconium button was used as an oxygen getter. The buttons obtained from the arc melting process were wrapped in tantalum foil, placed in evacuated quartz tubes, annealed at 900 °C for 12 days, and cooled down to room temperature by quenching in cold water. Overall mass loss after the melting and annealing processes were negligible (≈1%).

The low-temperature experiments were performed with a Quantum Design Physical Properties Measurements System (PPMS) allowing for the application of a magnetic field as large as 9 T. Thin Pt wires (ϕ = 37 μm) serving as electrical contacts for transport and Hall measurements were spark welded to the polished sample surface. A standard four-probe contact configuration was used to measure resistivity. A magnetic field was applied perpendicularly to the current direction. The Hall voltage was collected in reversal directions of magnetic field in order to remove the parasitic longitudinal magnetoresistance voltage due to misalignment of electrical contacts. The specific-heat measurements were performed using the dual slope method on flat polished samples. Magnetization measurements were carried out using the ac/dc magnetometry system (ACMS) option of the PPMS system. Pieces of the samples were fixed in standard polyethylene straw holders.

III. RESULTS AND DISCUSSION

The phase composition and crystallographic structure of the samples were checked by powder x-ray diffraction (pXRD) at room temperature. The pXRD analysis shows that all observed

*Corresponding author: kamkolin@pg.edu.pl
†Corresponding author: tomasz.klimczuk@pg.edu.pl

TABLE I. Lattice constants, unit cell volumes, and the parameters of the LeBail refinements for $CeNiC_2$, $PrNiC_2$, and $NdNiC_2$, at room temperature.

	$CeNiC_2$	$PrNiC_2$	$NdNiC_2$
a (Å)	3.8753(2)	3.8239(5)	3.7834(1)
b (Å)	4.5477(2)	4.5428(8)	4.5361(1)
c (Å)	6.1601(3)	6.1448(1)	6.1285(1)
V (Å^3)	108.565(8)	106.746(3)	105.178(3)
R_p	12.3	7.51	8.35
R_{wp}	16.5	10.1	10.8
$R_{\exp}$	11.49	7.54	7.7
χ^2	2.05	1.81	1.96

peaks for $NdNiC_2$ and $PrNiC_2$ are successfully indexed in the orthorhombic $CeNiC_2$-type structure [42] with a space group $Amm2$ (#38), which confirms the phase purity of the obtained samples. Only for the $CeNiC_2$ sample, the additional reflections corresponding to a small amount of the secondary phase [44] CeC_2 are observed. The lattice parameters were determined from the LeBail profile refinements of the pXRD patterns carried out using FULLPROF software [45]. The obtained values of the lattice constants, shown in Table I, are in good agreement with those reported in the literature [39,43,46,47].

The temperature dependence of the magnetic susceptibility (χ) measured at 1 T applied magnetic field is presented in Fig. 1. All three compounds show paramagnetic behavior at high temperatures. The $\chi(T)$ data were fitted using the modified Curie-Weiss expression

$$\chi(T) = \frac{C}{T - \Theta_{CW}} + \chi_0, \tag{1}$$

where C is the Curie constant, Θ_{CW} is the Curie-Weiss temperature, and χ_0 is the temperature-independent susceptibility resulting from both sample (Pauli and Van Vleck paramagnetism, Landau diamagnetism) and sample holder (small diamagnetic contribution of sample straw assembly). Having estimated the C parameter and assuming that the magnetic moment originates from R^{3+} ions only, one can calculate the effective magnetic moment using the relation shown in Eq. (2),

$$\mu_{\text{eff}} = \sqrt{\frac{3Ck_B}{{\mu_B}^2 N_A}}, \tag{2}$$

where k_B is the Boltzmann constant, μ_B is the Bohr magneton, and N_A is Avogadro's number. The resulting effective magnetic moments of $CeNiC_2$, $PrNiC_2$, and $NdNiC_2$ are consistent with the values expected for free R^{3+} ions [48]. The negative sign of Θ_{CW} obtained for the Ce- and Nd-bearing compounds (-26 K and -5.9 K, respectively) indicate an effectively antiferromagnetic coupling between the magnetic moments. In the case of $PrNiC_2$, the absolute value of Θ_{CW} is close to 0, suggesting the weakness or absence of magnetic interactions down to 2 K.

It is worth noting that the measured susceptibility of $PrNiC_2$ is well reproduced by the modified Curie-Weiss equation, yielding reasonable values of C, Θ_{CW}, and χ_0 and suggesting that the contribution of Pr^{3+} local moments is the dominant part of magnetic susceptibility above 35 K. The Van Vleck paramagnetic contribution reported by Onodera *et al.* [43] is in our case well modeled by the temperature-independent term χ_0.

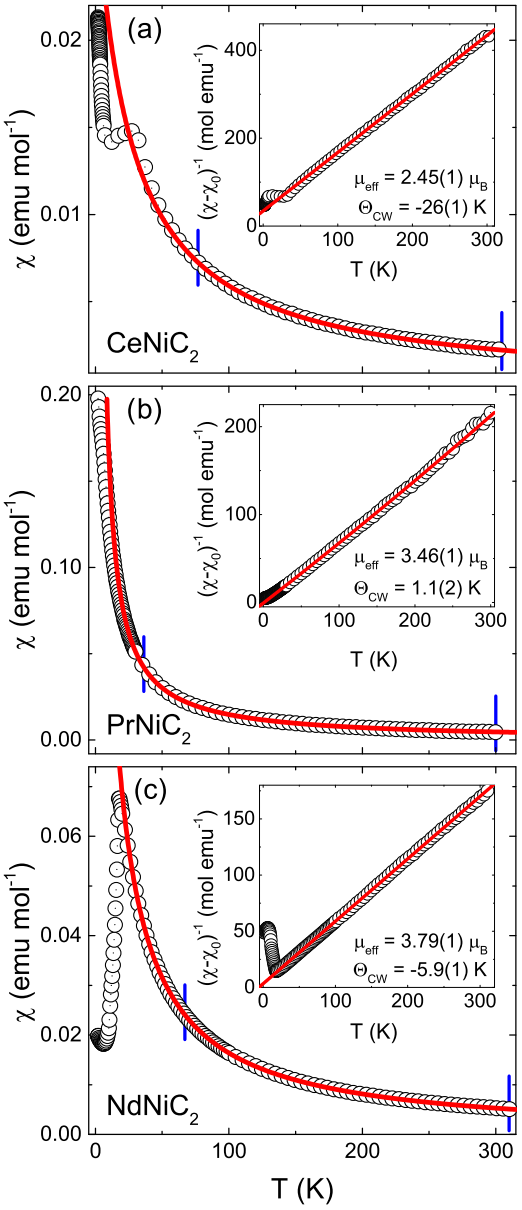

FIG. 1. Magnetic susceptibility of $CeNiC_2$ (a), $PrNiC_2$ (b), and $NdNiC_2$ (c) at applied magnetic field $\mu_0 H = 1$ T (open circles). Red lines show fits using the modified Curie-Weiss expression [Eq. (1)]. Insets show inverse susceptibilities displaying linear temperature dependence in agreement with the Curie-Weiss law [Eq. (1)]. Blue ticks mark the used fitting ranges. The effective magnetic moments extracted from fits agree with the values expected for free trivalent R ions. The low-temperature part of susceptibility for $PrNiC_2$ is presented in Fig. 2.

Upon crossing the Néel temperature $T_N = 17$ K, the magnetic susceptibility of $NdNiC_2$ drops rapidly. A similar drop, yet much less pronounced, is seen also in $CeNiC_2$ below $T_N = 19$ K. The susceptibility of $PrNiC_2$ shows no clear sign of a magnetic transition above 2 K, in agreement with previous reports [37,43]. The expanded view of ac magnetic susceptibility in $PrNiC_2$ at the low temperature shown in Fig. 2

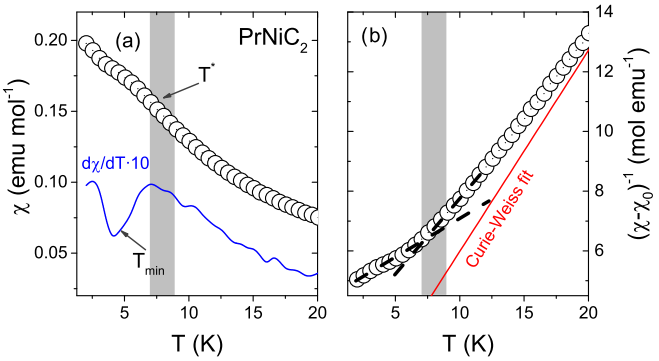

FIG. 2. (a) Low-temperature dc magnetic susceptibility of $PrNiC_2$ measured at 1 T applied field showing a slight upturn around 7 K, below the magnetic anomaly temperature T^* (see text). The differential of the dc susceptibility (blue line) shows a minimum around 4 K. (b) Inverse magnetic susceptibility of $PrNiC_2$ corrected for the temperature-independent contributions χ_0. The red line shows the Curie-Weiss fit from Fig. 1(b). Dashed lines are a guide for the eye.

reveals a small kink in the curve is seen at $T^* \approx 8$ K, consistent with the decrease in magnetization along the *a* crystallographic axis seen at this temperature by Onodera *et al.* [43]. The underlying cause for this magnetization anomaly is not clear, but may suggest some type of electronic or crystal structure transition, resulting in the decrease of Pauli or Van Vleck paramagnetic susceptibility.

Magnetization vs applied field [$M(H)$] for $CeNiC_2$, $PrNiC_2$, and $NdNiC_2$ is presented in Fig. 3. For $CeNiC_2$ [Fig. 3(a)] the magnetization is linear above T_N, with an upturn developing above approximately 4 T in the lower temperatures. Below the second transition temperature ($T_t = 7$ K) hysteresis is observed in $M(H)$. Even at 9 T applied magnetic field, the magnetization reaches only $0.27\mu_B$, which is approximately 13% of the expected saturation magnetization for Ce^{3+} ion $gJ = 2.14\mu_B$ (where $g = \frac{4}{5}$ is the Lande g factor, and $J = 4$ is the total angular momentum) [48]. The magnetization at 2 K and 9 T for $CeNiC_2$ is, however, approximately half of the observed saturation moment for a pure Ce metal, which is only $0.6\mu_B$ [48].

For $PrNiC_2$, $M(H)$ is roughly linear up to 9 T applied field at temperatures above 40 K [see Fig. 3(b)], below which the curves start to slightly deviate from linearity. At 10 K and below [Fig. 3(b), inset] the deviation is more pronounced and the curves start to saturate. At 2 K and 9 T applied field the $M(H)$ of $PrNiC_2$ reaches approximately $1.5\mu_B$, which is half of the expected saturation magnetization for Pr^{3+} ion $gJ = 3.20\mu_B$ [48].

In case of $NdNiC_2$, the magnetization curves are linear down to 20 K [Figs. 3(c) and 3(d)]. Below the T_N the [$M(H)$] is strongly suppressed, but above 4 T a sudden upturn is observed, resulting from field-induced magnetic order-order transition that reduces the AFM compensation of local moments. Similar transitions have been previously observed in $GdNiC_2$ [49]. Above the transition the $M(H)$ curves start to saturate, reaching $1.6\mu_B$ in 9 T at 2 K, about one half the saturation magnetization for the Gd ion ($gJ = 3.27\mu_B$ [48]). The magnetization loop shows no trace of hysteresis at the AFM-FM transition as it is presented in the inset of Fig. 3(c).

The real part of the ac magnetic susceptibility of $CeNiC_2$ and $NdNiC_2$ shows a drop at the Néel temperature T_N of 19 K and 17 K, respectively [see Figs. 4(a) and 4(c)], in agreement with previous reports [43]. Below T_N both compounds undergo further magnetic transitions. In $CeNiC_2$ a sudden drop of susceptibility is seen at $T_t = 7$ K, followed by a pronounced upturn. The change in magnetic order below 10 K was previously observed by magnetization, specific-heat, and NMR measurements [43,46]. An additional small upturn around 29 K results from the presence of a minor quantity of the antiferromagnetic CeC_2 impurity phase [44] ($T_N = 30$ K), observed in XRD measurements. In $NdNiC_2$ a small feature is seen around 4 K [see the inset of Fig. 4(c)] that was reported by Onodera *et al.* [43]. The ac susceptibility of $PrNiC_2$ shows no clear sign of magnetic transition; however, the slightly saturating dependency of χ' and its derivative $d\chi'/dT$ resembles the results obtained for the $Pb_2Sr_2PrCu_3O_8$ compound in which a quasi-2D magnetic order is observed below 7 K, as evidenced by neutron diffraction study [50]. In the aforementioned case the ac susceptibility shows a saturation below the ordering temperature rather than a pronounced drop, while the differential exhibits a minimum at the ordering temperature. In our case there is no clear minimum of the differential curve, yet it would be necessary to perform a neutron diffraction measurement in order to confirm or deny the presence of long-range magnetic order below the T^*.

In contrast with $CeNiC_2$ and $NdNiC_2$, $PrNiC_2$ does not reveal any clear magnetic transition. Since the three compounds are chemically similar, the discrepancy arises likely from the difference in the detailed structure of $4f$ energy levels. The ground state of a free Pr^{3+} ion is ninefold degenerate with total angular momentum $J = 4$. The crystalline electric field (CEF) acting on the Pr^{3+} removes the degeneracy (either fully or partially), with the nature of the effect dependent on the point symmetry of the ion crystallographic position. In the orthorhombic $PrNiC_2$ the $2a$ site occupied by a Pr atom has the point symmetry group $mm2$. For such relatively low symmetry one would expect a complete uplifting of the ground-state degeneracy, yielding a nonmagnetic configuration with nine separated singlet states similarly as in $PrNi_2Al_5$ [51]. Note, however, that in the case of exchange interaction energy exceeding the first CEF excitation, the magnetic order may appear due to the intermixing of higher energy states into a ground state with higher degeneracy [52]. Such situation occurs in the orthorhombic $PrNiGe_2$ compound crystallizing in the $CeNiSi_2$-type structure (related to $CeNiC_2$) in which the Pr^{3+} ion position has the same point symmetry as in $PrNiC_2$, yet the material reveals ferromagnetic (FM) ordering at $T_C = 13$ K [52,53].

Figures 5(a)–5(c), show the thermal dependencies of electrical resistivity (ρ_{xx}), measured without and with applied magnetic field (9 T), for $CeNiC_2$, $PrNiC_2$, and $NdNiC_2$, respectively. At high temperatures, all the compounds exhibit typical metallic behavior with resistivity deceasing with temperature lowering. Upon cooling, ρ_{xx} of both $PrNiC_2$ and $NdNiC_2$ show the anomalies pronounced by a minimum followed by a hump. This metal-metal transition is a typical signature of the charge density wave state with incomplete Fermi surface nesting,

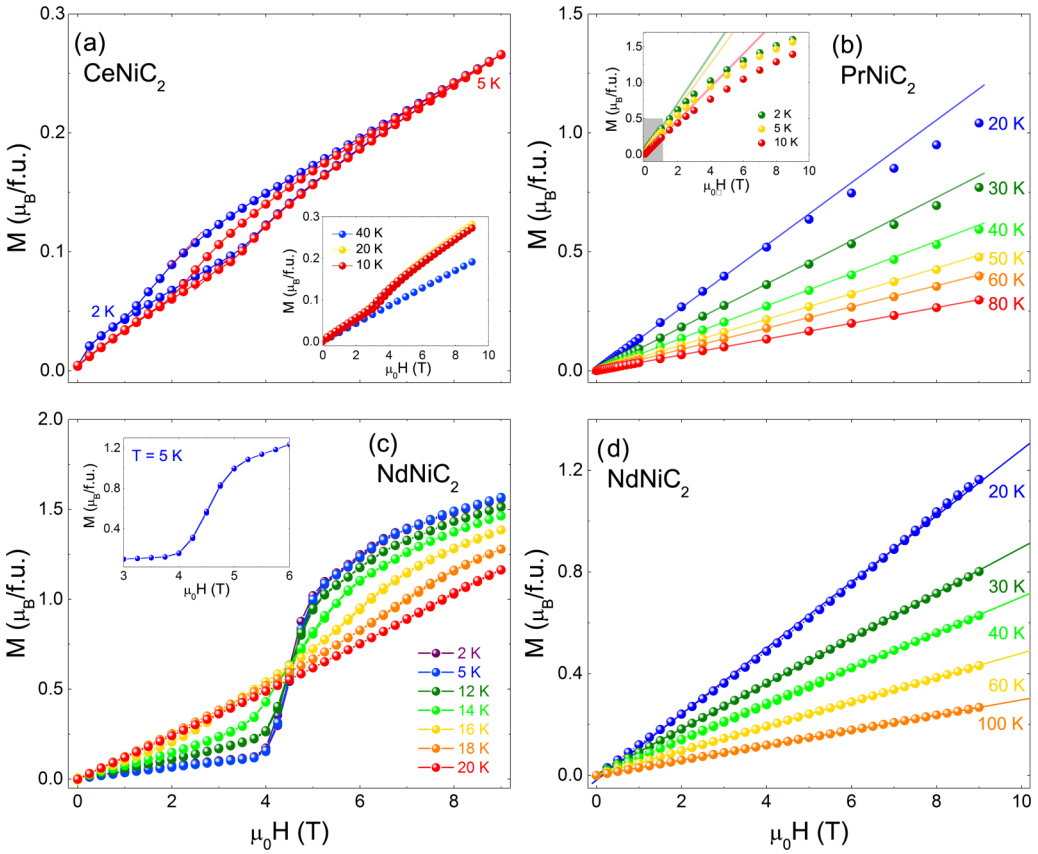

FIG. 3. (a) Magnetization vs applied magnetic field [$M(H)$] measured for $CeNiC_2$ at 2 K and 5 K (below the Néel temperature $T_N = 19$ K) showing a hysteretic behavior probably due to a field-induced magnetic transition. The inset presents the magnetization at 10 K, 20 K, and 40 K. While the magnetization at $T \geqslant 40$ K (above the AFM transition) is a linear function of applied field, in the vicinity (20 K) and below the T_N an upturn is seen around 3 T, suggesting the field-induced magnetic transition suppressing the AFM order. (b) $M(H)$ curves for $PrNiC_2$ showing linear character down to 40 K. Below that temperature the curves start to saturate in high magnetic fields. At the lowest temperatures (2 K, 5 K, and 10 K; see inset) the deviation from linearity is clear above 1–2 T. Straight lines are least-squares linear fits to the low-field (below 1 T) magnetization data. Gray shading in the inset marks the fitting range used. (c) The low-temperature $M(H)$ data for $NdNiC_2$. At 20 K (above the $T_N = 17$ K) the curve is linear up to 9 T, while below this temperature an upturn is observed above approximately 4 T. In the temperatures lower than T_N the magnetization below approximately 4 T is visibly suppressed due to AFM ordering of the magnetic moments. At 4 T a magnetic order-order transition results in rapid increase in magnetization. The inset shows magnetization around the field-induced magnetic transition at 5 K showing no sign of hysteresis. (d) Magnetization of $NdNiC_2$ between 20 K and 100 K, showing a linear character up to 9 T. Straight lines are least-squares linear fits to the low-field data.

characteristic for quasi-2D materials [54]. The temperature of this anomaly corresponds to the Peierls temperature ($T_P = 121$ K for $NdNiC_2$ and $T_P = 89$ K for $PrNiC_2$) established by x-ray diffuse scattering [28]. In contrast to that, no CDW-like anomaly is observed in the third compound, $CeNiC_2$. At the magnetic crossover temperatures, all three curves exhibit a decrease in resistivity, shown closer in the insets of Fig. 5. This downturn is visibly sharper for the antiferromagnetic ground states of $NdNiC_2$ and $CeNiC_2$ than in the case of $PrNiC_2$, where instead of a long range of magnetic ordering, one observes a small magnetic anomaly at T^*.

Although the anomalies in the zero-field resistivity have been reported beforehand [27], the influence of magnetic field on transport properties, up to now, has been studied solely for the Nd-bearing compound [28,55]. Electrical resistivity measured in the presence of a magnetic field of $\mu_0 H = 9$ T is shown as a red line in Figs. 5(a)–5(c). The influence of magnetic field on ρ_{xx} in the high-temperature metallic state of each compound is negligibly small. In $CeNiC_2$, this behavior is present down to the vicinity of T_N, where the magnetic field weakly modifies the resistivity. This is in contrast to the features seen in the two compounds exhibiting the charge density waves; in $NdNiC_2$ one observes a notable decrease in resistance with magnetic field at $T \to T_N$. In $PrNiC_2$ the onset of the negative magnetoresistance can be observed at $T \approx 60$ K, much closer to T_P than in $NdNiC_2$. To investigate further the impact of $\mu_0 H$ on transport properties of studied compounds, we have performed the field sweeps at constant temperatures.

The magnetic-field dependence of magnetoresistance [$\mathrm{MR} = \frac{\rho(H)-\rho_0}{\rho_0}$, where ρ_0 is the zero-field resistivity] of $CeNiC_2$ is depicted in Fig. 6(a). At $T > T_N$, MR is weak and negative (resistivity decreases by a maximum of 3%). Below this temperature, the magnetoresistance changes its sign and magnitude. This is a typical picture of the modification of the scattering rate in the vicinity of the magnetic ordering temperature [56–58]; above T_N the reduction of resistance can

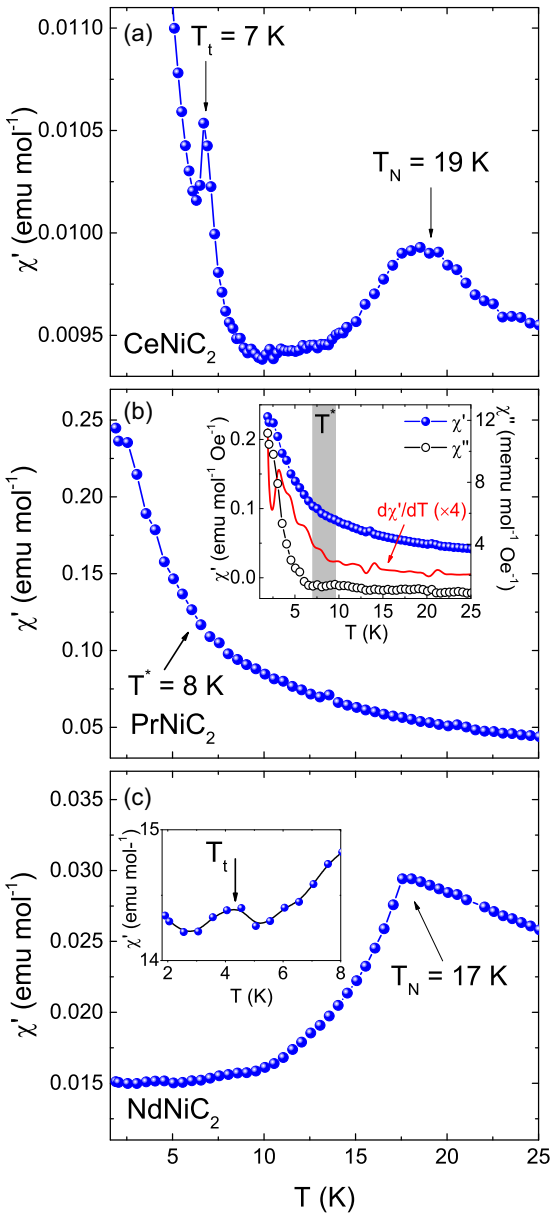

FIG. 4. Real part of ac magnetic susceptibility of (a) $CeNiC_2$, (b) $PrNiC_2$, (c) $NdNiC_2$ measured in a constant field of 5 Oe with 3 Oe, 1 kHz excitations. Arrows on panel (a) indicate the transition to an AFM state at $T_N = 19$ K and order-order transition at approximately 7 K. The inset of panel (b) presents the comparison of real and imaginary parts of the ac susceptibility (blue and black points, respectively) and the derivative of the real part (red line). The value of the derivative is negative and decreases with decreasing temperature. In panel (c) the $T_N = 17$ K is defined as a position of the drop of susceptibility at the AFM transition. The inset shows a small jump around 4 K that is attributed to magnetic order-order transition.

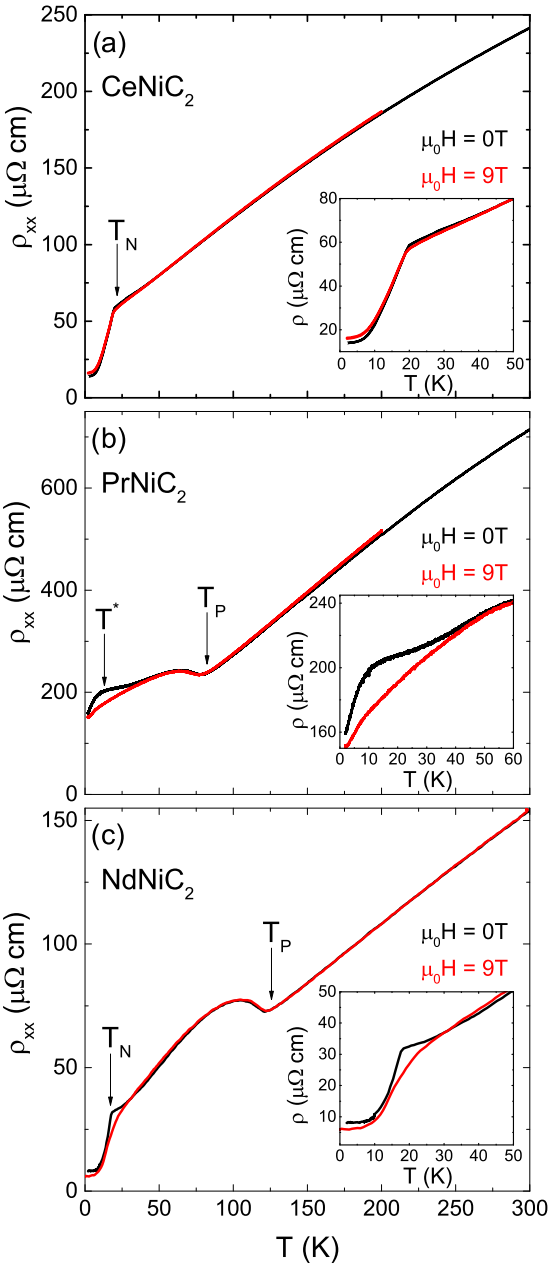

FIG. 5. Resistivity of (a) $CeNiC_2$, (b) $PrNiC_2$, (c) $NdNiC_2$, measured without (black color) and with (red color) applied magnetic field of 9 T. Arrows indicate characteristic temperatures: T_P, Peierls temperature for $NdNiC_2$ and $PrNiC_2$; T_N, Néel temperature for $CeNiC_2$ and $NdNiC_2$; and T^*, magnetic anomaly temperature in $PrNiC_2$. (Insets) Expanded view of the vicinity of the magnetic ordering (anomaly) temperature.

be attributed to the field-induced ordering of the local magnetic moments, resulting in the quenching of the spin fluctuations and effectively a decrease of the related scattering mechanism. On the other side of the transition, below T_N, the magnetic field induces a partial reorientation of the local spins and perturbs the antiferromagnetic order, which results in the increase of the scattering rate and, consequently, of the electrical resistance.

Figure 6(b) shows the magnetic-field dependence of magnetoresistance of $PrNiC_2$. One can notice that, in the charge density wave state, MR is dominated by the negative component which rises as temperature decreases down to T^*. Below this temperature limit, the negative MR decreases, and finally at $T = 2$ K a positive term can be observed at low magnetic field. This positive MR component can originate from an onset of another magneticlike transition at lower temperatures or from the light carriers related to the small Fermi surface

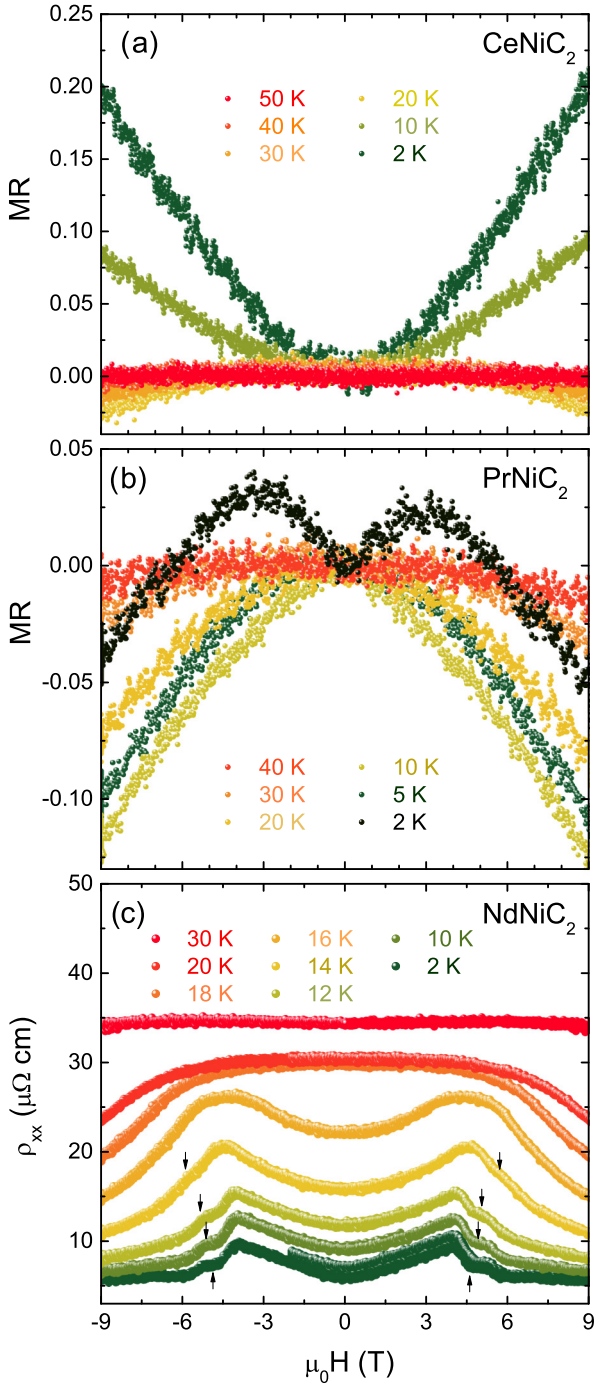

FIG. 6. Magnetotransport properties of $R\mathrm{NiC_2}$. All the measurements have been performed at constant temperature. (a) Magnetoresistance in $\mathrm{CeNiC_2}$ as a function of magnetic field. (b) Magnetic-field dependence of magnetoresistance in $\mathrm{PrNiC_2}$. (c) Resistivity of $\mathrm{NdNiC_2}$ as a function of magnetic field. For better clarity, for this compound we show the ρ_{xx} instead of MR. Arrows indicate the kinks attributed to a metamagnetic phase separating the FM and AFM orders.

pockets that can be opened in the FS due to imperfect nesting. A complementary experiment, such as angle-resolved photoemission fine-structure spectroscopy, neutron diffraction, or magnetotransport measurements performed at temperatures below 1.9 K and higher field, would be required to clarify this point. Figure 6(c) shows the magnetic-field dependence of resistivity of $\mathrm{NdNiC_2}$. Due to the rich variety of positive and negative MR components seen in this compound, we find it more clear to use the $\rho_{xx}(H)$ instead of MR(H) for discussion of the magnetotransport properties in $\mathrm{NdNiC_2}$. At 30 K, one observes an onset of the negative magnetoresistance term, which becomes stronger as temperature decreases. Below T_N, the resistivity first rises with magnetic field and after reaching the maximum, the ρ_{xx} decreases again. The position of the resistivity maximum at various temperatures below T_N corresponds to the magnetic-field-induced ferromagnetic transition according to the H-T phase diagram of $\mathrm{NdNiC_2}$ constructed for a single crystal [43]. Below 14 K, one observes an additional kink (marked by arrows in Fig. 6) on the decreasing side of resistance. This can be attributed to the intermediate magnetic phase separating the AFM and FM orders at this temperature range. In addition, one can notice that at the lowest temperatures the resistivity saturates at high magnetic fields. The negative magnetoresistance in $\mathrm{NdNiC_2}$ has been attributed [28,55] both to the suppression of spin disorder scattering and to the destruction of the charge density wave, as seen in the isostructural, albeit ferromagnetic compound, $\mathrm{SmNiC_2}$, in which the relevance of the CDW suppression has been confirmed by the x-ray diffuse scattering experiment performed in magnetic field [59,60].

An interesting observation is the irreversible behavior of the electrical resistivity at low temperatures. In order to prove that this effect is not an artifact caused by unstable electrical contacts and is intrinsic to the sample, we have repeated the measurement at lower temperatures. First, the sample was warmed up to 40 K, far above the magnetic ordering temperature ($T_N = 17$ K). Next, we have cooled the sample with zero applied field and stabilized the temperature before activating the magnet. The magnetic field was swept initially to 2 T to avoid crossing the AFM-FM transition. Then, the magnetic field was swept and reached -9 T (9 T applied in the adverse direction). Afterwards, we performed the final sweep and continuously reversed the direction of the magnetic field to 9 T. The whole procedure was repeated for each scan in order to remove any magnetic memory from the sample. In Fig. 7 we show the results of the field sweeps at the selected temperatures.

The resistivity measured at $T = 14$ K [Fig. 7(a)] is reversible with $\mu_0 H$. At $T = 10$ K [Fig. 7(b)] one can notice a small irreversibility of ρ_{xx}, which becomes more pronounced at $T = 8$ K, as depicted in Fig. 7(c). When the magnetic field is increased to 2 T and then swept to 0, the resistivity returns to the zero-field cooled (ZFC) value of ρ_0. Under these conditions, the sample remains in the AFM state. However, the application of a magnetic field exceeding the limit of 4 T, at which the FM order is induced in the sample, prevents the resistance from returning to the original ρ_0. Further magnetic field sweeps do not induce any irreversible transitions, and the resistivity returns to the new value of ρ_0^* when the field is reduced back to 0. Figure 7(d) compares the result of a field sweep of the sample cooled to 2 K in ZFC condition and the ρ_{xx} of the same sample, which previously experienced the transformation to the FM state at $T = 5$ K (inset). The irreversible behavior is clearly visible in the former case, while in the latter one the resistivity returns to the initial value. This shows that the resistance of $\mathrm{NdNiC_2}$ depends not only on

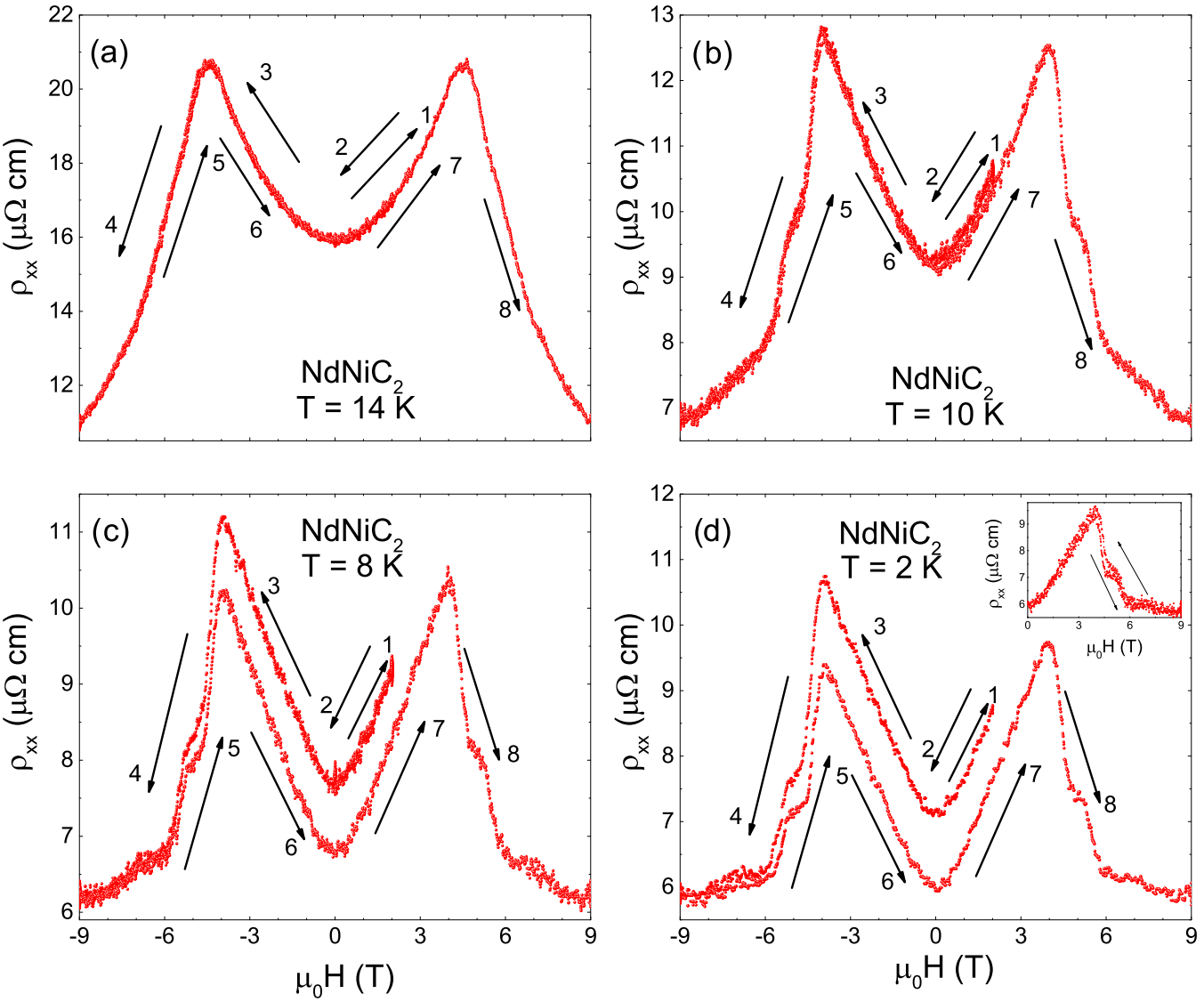

FIG. 7. Resistivity of $NdNiC_2$ measured at selected temperatures. After each field sweep data collection at constant temperature, the sample was warmed up to 40 K in zero magnetic field to remove the magnetic memory of the material. Arrows and numbers show the direction of field sweeps. (a) $T = 14$ K; (b) $T = 10$ K; (c) $T = 8$ K; (d) $T = 2$ K. (Inset) Resistivity at $T = 2$ K of the same sample of $NdNiC_2$, however, previously subjected to the magnetic field of 9 T at $T = 5$ K.

temperature, applied magnetic field, or the type of magnetic ordering present in the sample at these conditions, but also on the magnetic history of the sample and this metastable effect is clearly associated with the AFM-FM transition. Previous reports on the magnetoresistance of $NdNiC_2$ [28,55] have not mentioned the irreversible phase transition, probably because this weak crossover could be easily overlooked, since once the sample experiences the high magnetic field at temperature below 12 K it remains in the metastable state and the irreversibility is no longer observable until the sample is reheated and cooled down again. One plausible scenario to explain this irreversible effect is the magnetoplastic lattice deformation induced by the ferromagnetic transition. Note that even a small lattice transformation and a consequent Fermi surface modification can substantially impact the nesting conditions, and this can lead to the quasipermanent suppression of CDW.

The BCS approach predicts the negative magnetoresistance in CDW systems to originate from the Zeeman splitting of the conduction bands [61], which results in reduction of the pairing interactions and degradation of nesting properties. This term has been found to originate both from orbital effects and from local spins producing stronger magnetic moments. For magnetic fields $\mu_B H \ll \Delta_{CDW}$, the Zeeman magnetoresistance term is expressed [8] by Eq. (3):

$$MR = \frac{\rho(H) - \rho_0}{\rho_0} = -\frac{1}{2}\left(\frac{\mu_B H}{k_B T}\right)^2 + 0\left(\frac{\mu_B H}{k_B T}\right)^4, \quad (3)$$

Figure 8(a) shows the magnetoresistance of $NdNiC_2$ above T_N as a function of $\frac{1}{2}\left(\frac{\mu_B H}{k_B T}\right)^2$. The plots do not converge into a single straight line. This is not surprising, since this temperature interval corresponds to the onset of the field-induced magnetic ordering. This can lead either to the pre-

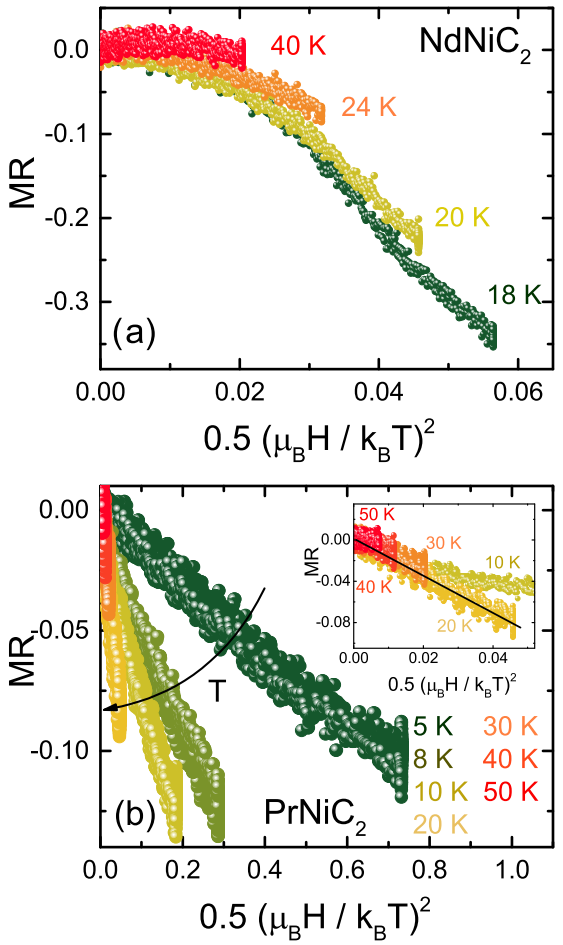

FIG. 8. Scaling of magnetoresistance in $PrNiC_2$ with Eq. (3). (Inset) Expanded view the MR scaling for $T \geqslant 10$ K.

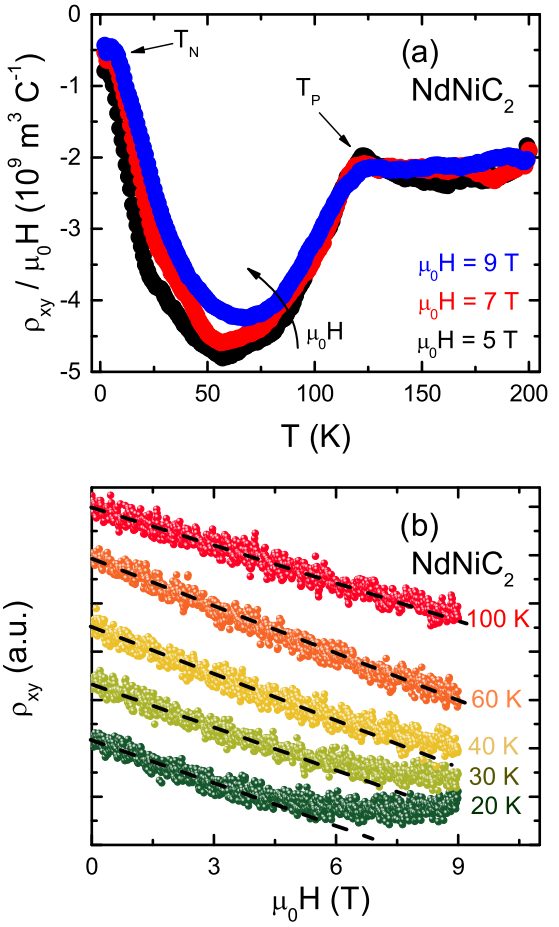

FIG. 9. (a) Hall resistivity of $NdNiC_2$, divided by magnetic field, measured at various magnetic fields. Arrows indicate the Peierls and Néel temperatures T_P and T_N, respectively. (b) Hall resistivity of $NdNiC_2$ as a function of magnetic field. The plots have been shifted horizontally to improve data reading.

viously suggested CDW suppression, stronger than predicted by Eq. (3), or to the reduction of the spin scattering, which also results in negative magnetoresistance as in $CeNiC_2$. The comparison of the strength of the negative magnetoresistance in $NdNiC_2$ and $CeNiC_2$ in the vicinity of T_N can also be a useful guide. In the former compound, showing the Peierls instability, MR reaches -40%, which is an order of magnitude larger than in the latter one, in which the CDW is absent. This suggests that the negative magnetoresistance in $NdNiC_2$ originates, at least partially, from the suppression of the CDW state.

The negative MR in $PrNiC_2$ reaches a maximum of 12%, which although is visibly weaker than in $NdNiC_2$, still exceeds the value found in $CeNiC_2$. This, similar to the case of $NdNiC_2$, suggests that the decrease of resistance in magnetic field originates from the suppression of the CDW. To verify this hypothesis, we have scaled the magnetoresistance in $PrNiC_2$ with Eq. (3), as shown in Fig. 8(b). At $T > 20$ K the $PrNiC_2$ can be qualitatively described by the Zeeman term; the MR plots fall into a single straight line. At lower temperatures, in the vicinity of T_M the negative magnetoresistance is weakened and diverges from this scaling law [as shown in the inset of Fig. 8(b)]. The curve obtained for $T = 10$ K is a boundary of the relevance of the Eq. (3). At $\frac{1}{2}\left(\frac{\mu_B H}{k_B T}\right)^2 \approx 0.02$, which corresponds to $\mu_B H = 6$ T at this temperature, the magnetoresistance plot diverges from the Zeeman scaling and starts decreasing. We find that to apply Eq. (3) one has to use the prefactor of approximately 1.4. In other CDW materials this coefficient is usually smaller than unity. The key examples are $Li_{0.9}Mo_6O_{17}$ [62] or organic compounds such as $(Per)_2Pt(mnt)_2$ [63–66] in which the existence of weakly magnetic chains ramps this magnetoresistance prefactor in comparison with $(Per)_2Au(mnt)_2$ [67,68] showing a nonmagnetic character. On the other hand, the value we found is significantly lower than the factor of ≈30 found in $GdNiC_2$ [49], where the presence of strong local magnetic moments amplifies the internal magnetic field much more effectively than in $PrNiC_2$, showing no clear long-range magnetic ordering.

Due to the polycrystalline nature of our samples, we are unable to perform the x-ray diffuse scattering experiment to follow the intensity and position of the satellite reflections at various temperatures and magnetic fields. Instead, to investigate the suppression of the charge density waves state by magnetic field, we have conducted the Hall effect measurements, which can be used as a direct probe for electronic carrier concentration. Figure 9(a) shows the thermal dependence of

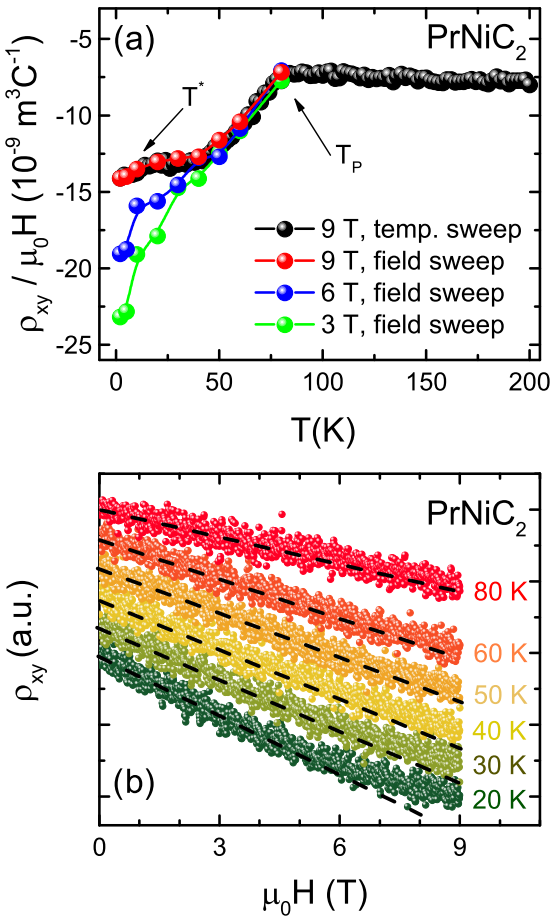

FIG. 10. (a) Hall resistivity of $PrNiC_2$, divided by magnetic field. Black points show the data collected from the temperature sweep at constant magnetic field of 9 T. Red, blue, and green points show the data collected from the field sweeps at constant temperature. Arrows indicate the Peierls and magnetic transition temperatures T_P and T^*, respectively. Solid lines are guides for the eye. (b) Hall resistivity of $PrNiC_2$ as a function of magnetic field. The plots have been shifted horizontally to improve data reading. Dashed lines show the low-field linear dependencies of $\rho_{xy}(H)$ expanded to the high-field regime.

Hall resistivity (ρ_{xy}) in $NdNiC_2$. The sign of the measured Hall resistance is negative, opposite to the results reported recently [55]. To clarify this point, we have repeated the measurement with a reference sample of Cu foil, which shows a negative Hall signal in the same contact geometry. This confirms the relevance of the negative sign of ρ_{xy} in $NdNiC_2$. At $T > T_P$, the Hall signal is almost independent of temperature. At the Peierls temperature one observes a downturn of $\rho_{xy}(T)$ (and increase of $|\rho_{xy}|$), which is a typical signature of the opening of the CDW band gap and condensation of electronic carriers [69,70]. Upon further cooling, the Hall resistivity decreases until it reaches a minimum followed by a prominent increase of ρ_{xy} (and decrease of $|\rho_{xy}|$), which grows even higher than for temperatures above T_P.

This increase of ρ_{xy} in proximity of the magnetic ordering temperature observed in $SmNiC_2$ [71] and $NdNiC_2$ [55] has been attributed to the destruction of CDW and a concomitant release of previously condensed carriers. Although the CDW suppression by magnetic field appears to be quite a possible scenario, this mechanism itself is not sufficient to explain the features observed as $T \to T_N$, especially considering that the low-temperature $|\rho_{xy}|$ is lower than the value found for $T > T_P$. This could lead to a misguiding suggestion that the carrier concentration below T_N exceeds the high-temperature normal-state value. To avoid the oversimplification, in a material exhibiting magnetic ordering, one has to consider two components of the Hall resistance [72]:

$$\rho_{xy} = R_0\mu_0 H + 4\pi R_S M. \tag{4}$$

The R_0 in Eq. (4) is the ordinary Hall coefficient which, in a single-band model, is inversely proportional to the carrier concentration. R_S denotes the anomalous Hall coefficient associated with side jump and skew scattering. To obtain the more clear evidence of the partial CDW destruction in $NdNiC_2$, we complement the previous Hall effect study [55] of this compound in regard to the anomalous component of the Hall signal. We also present the results of the same experiment for $CeNiC_2$ and $PrNiC_2$, which, similarly to magnetoresistance in these two compounds, have not been reported previously. The separation of normal and anomalous ρ_{xy} components is not straightforward unless the magnetic moment saturates with magnetic field, which then reduces the latter one to a constant [73–76]. Here, no signs of saturation of $M(T)$ up to an applied field of 14 T for any of the studied compounds have been found [77], which precludes the possibility of the direct extraction of electronic concentration from ρ_{xy}. Nevertheless, we can propose an alternative road to follow the number of carriers condensed into the charge density wave state. The idea is to compare the field dependencies of ρ_{xy} and M with a special regard for the temperature region, in which magnetization follows the linear field dependency. Under this condition the anomalous component contribution is also linear with field and, for a single-band metal, any departure from the the linearity of ρ_{xy} indicates the change of R_0, which is a measure of electronic concentration.

Figure 9(b) shows the magnetic-field dependence of the Hall resistivity of $NdNiC_2$ measured at various temperatures. At $T \geqslant 60$ K one cannot find any departure from linearity

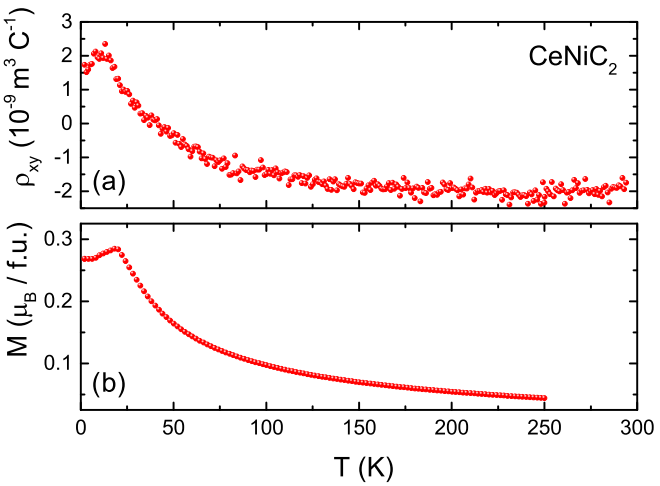

FIG. 11. Hall resistivity in $CeNiC_2$ as a function of temperature (a) compared with magnetization (b) of the same compound.

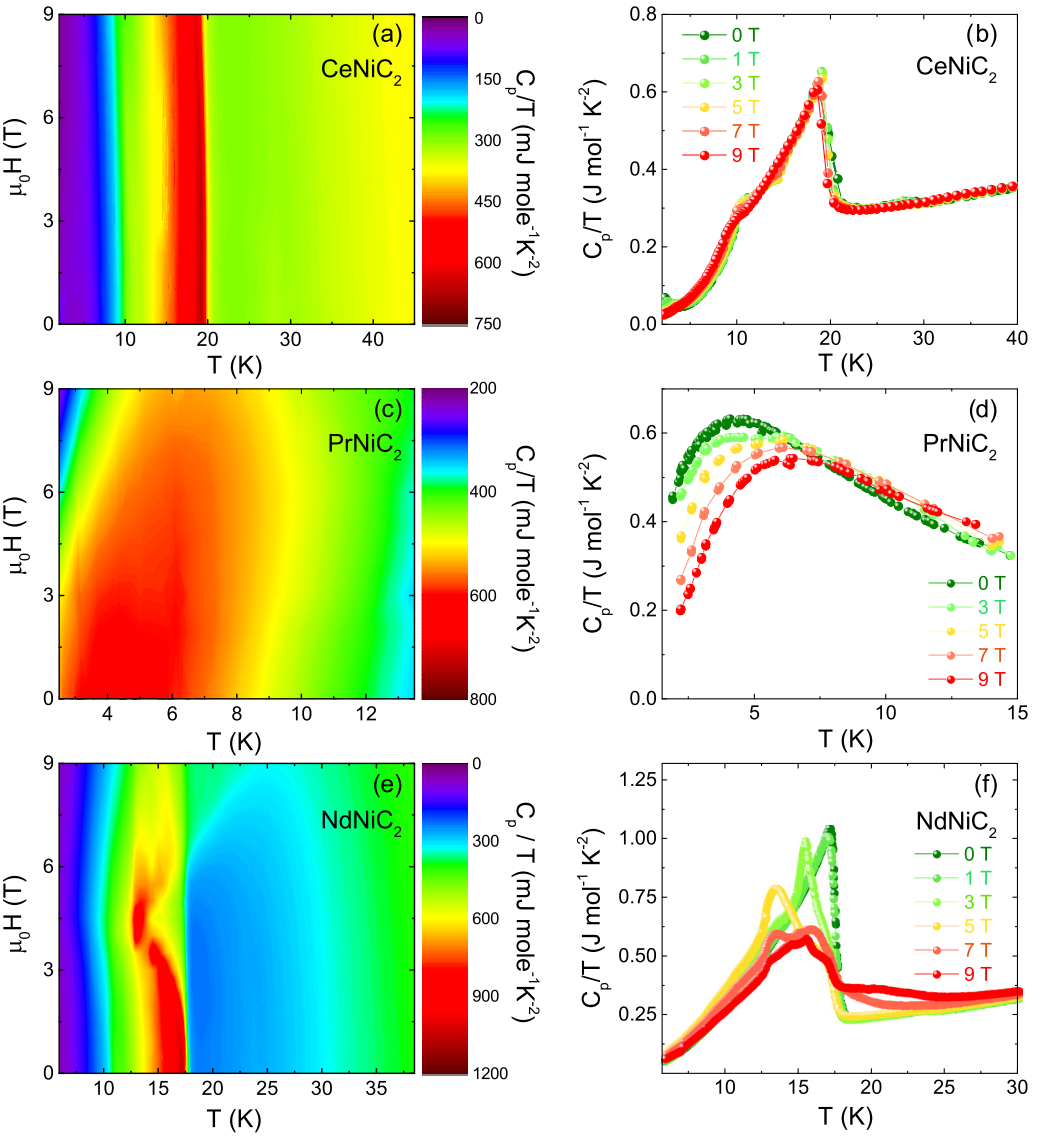

FIG. 12. Panels (a) and (b) present the specific heat of $CeNiC_2$ as a function of temperature and magnetic field. The anomaly seen at $T_N = 19$ K does not significantly shift with applied magnetic fields up to 9 T, while the anomalies around 10 K and 2 K are suppressed by increasing $\mu_0 H$. Panels (c) and (d) show the specific heat of $PrNiC_2$, revealing that the broad hump, attributed to the Schottky anomaly resulting from splitting of the f orbital energy levels is gradually shifted towards higher temperatures by application of a magnetic field due to the Zeeman effect. Panels (e) and (f) present the specific heat of $NdNiC_2$. The anomaly at 17 K remains almost unaffected by magnetic fields up to approximately 3 T, above which a field-induced magnetic transition takes place, as evidenced by magnetization and transport measurements. At higher fields the specific-heat curves develop a complicated structure, indicating that the magnetic phase diagram is complex, as previously reported for $GdNiC_2$ [49].

for the $\rho_{xy}(H)$. A small nonlinearity can be seen at 40 K. Upon further cooling, the deviation from linear variation for $\rho_{xy}(T)$ becomes more pronounced. Comparing this result with magnetization data for $NdNiC_2$ [Fig. 3(d)], which shows linear $M(H)$ dependence at $T \geqslant 20$ K, one can deduce that, in this temperature range, the nonlinearity of $\rho_{xy}(H)$ can be safely attributed to the increase in electronic concentration. This indicates that the release of previously CDW condensed carriers is, next to the anomalous Hall component, responsible for the increase of ρ_{xy} as temperature is lowered to the vicinity of T_N. Here we emphasize that, since we have not observed the saturation of $M(H)$, we are unable to separate the normal and anomalous components of the Hall resistivity for $T \leqslant 20$ K, where both ρ_{xy} and M are nonlinear functions of $\mu_0 H$.

The thermal dependence of Hall resistance of $PrNiC_2$ depicted in Fig. 10(a) exhibits some similarities to the case of $NdNiC_2$. A significant downturn of ρ_{xy} below T_P concomitant with an increase of resistivity [Fig. 5(c)] due to the condensation of the electronic carriers is observed at T_P. Upon further cooling, the Hall resistivity continues to decrease and does not simply saturate at $\frac{T_P}{2}$, where the electronic gap is expected to be fully open. This behavior is consistent with the non-BCS thermal dependence of the satellite reflections intensity [28], suggesting that the nesting vector adjusts to the FS evolution. In contrast to $NdNiC_2$, no significant upturn of ρ_{xy} is observed as

T approaches the magnetic ordering temperature. Contrarily, below T^* the Hall resistivity starts to decrease again. This observation is in agreement with the behavior of the intensity of the CDW satellite reflections [28], which show a sudden increase upon crossing T^*. Below $T \approx 60$ K, corresponding to the onset of negative magnetoresistance, the $\rho_{xy}(T)$ curves obtained at different magnetic fields do not converge. The application of stronger magnetic field drives the thermal dependence of ρ_{xy} towards more positive values, in comparison to the data obtained at lower H. Similar to $NdNiC_2$, this can be attributed to the positive anomalous Hall component growing as the magnetization increases or to the partial suppression of the CDW and the increase of the electronic concentration. It shall be noted that the strength of the ρ_{xy} downturn below T^* is sufficient to overcome the anomalous term driving the Hall resistivity towards more positive values. Note that the strength of the anomalous Hall signal in $PrNiC_2$ is expected to parallel the scale of $NdNiC_2$, since the values of magnetization of both compounds are comparable.

To explore this effect further, we have conducted $\rho_{xy}(H)$ measurements for $PrNiC_2$. As shown in Fig. 10(b), the nonlinearity of the Hall resistivity plotted versus $\mu_0 H$ can be observed in this compound as well. The deviation from linearity, initially barely observable for $T = 50$ K becomes stronger at lower temperatures. Here, however, we cannot follow the same analysis as for the case of $NdNiC_2$, due to the fact that for temperatures lower than 60 K the magnetization does not follow a linear relationship with $\mu_0 H$. Therefore, the two normal and anomalous ingredients of the Hall resistivity in $PrNiC_2$ cannot be unambiguously separated. Nevertheless, the downturn of ρ_{xy} at T^* strongly suggests the enhancement of the CDW state, although the magnetoresistance above T^* shows some signatures of the partial suppression of the Peierls instability. This can be explained in terms of the lattice transformation accompanying the magnetic anomaly modifying the Fermi surface, which triggers the nesting of another FS part when the CDW vector adjusts to band-structure evolution. One cannot, however, exclude an alternative scenario, in which the enhancement of the Fermi surface nesting can be seen as a driving force for the magnetic anomaly. Since the magnetic properties are related to the free-electron density via RKKY interactions, it is not unreasonable to expect the condensation of the electronic carriers at T^* to modify the magnetic character of $PrNiC_2$. The high-resolution x-ray and neutron diffraction experiment performed with a single crystal of $PrNiC_2$ will be required to clarify this point.

The thermal dependence of Hall resistivity in $CeNiC_2$, shown in Fig. 11(a), shows no signatures of electronic condensation. This is in agreement with transport properties in which no anomalies similar to those found in $NdNiC_2$ and $PrNiC_2$ are observed and confirms the absence of the Peierls instability in $CeNiC_2$. From the clear correlation between the thermal dependence of ρ_{xy} and magnetization [see Fig. 11(b)], one can conclude that the anomalous component is the dominant ingredient of the Hall effect in this compound, while the normal Hall coefficient is expected to remain temperature independent. The observation of the increase of ρ_{xy} as $T \rightarrow T_N$ in $CeNiC_2$, where the absence of the CDW has been emphasized, implies that the anomalous Hall component is essential to describe the ρ_{xy} in $NdNiC_2$ and $PrNiC_2$.

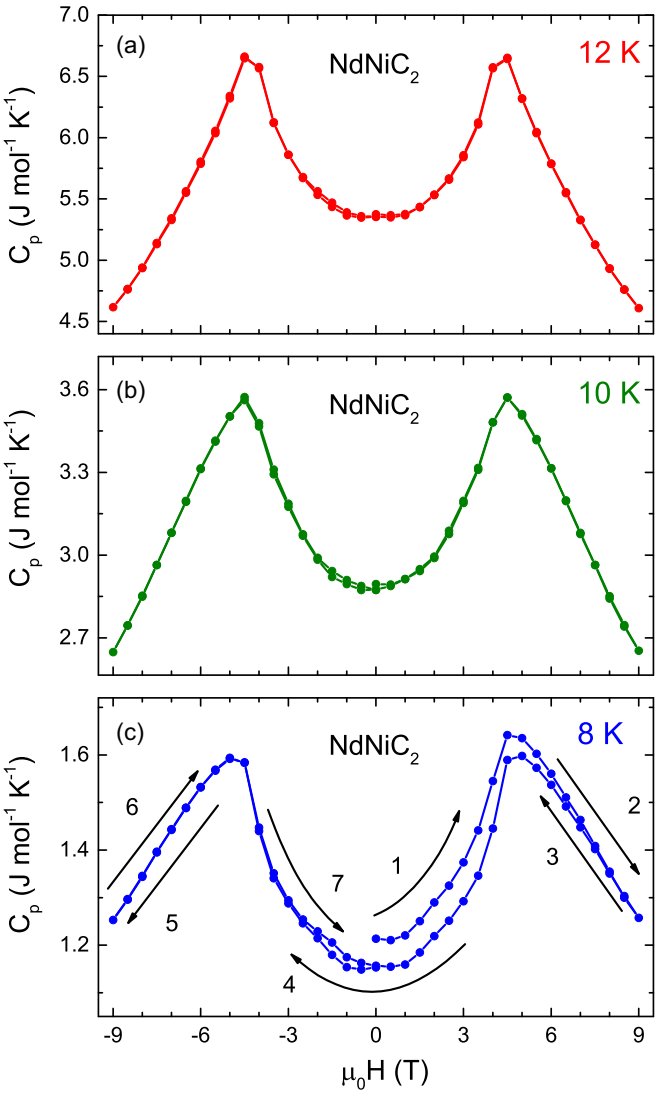

FIG. 13. Specific heat of $NdNiC_2$ as a function of magnetic field measured at (a) $T = 12$ K, (b) $T = 10$ K, and (c) $T = 8$ K. Arrows and numbers show the direction of the magnetic-field sweeps. At each temperature step the sample was first heated to 40 K, well above the magnetic transition temperature $T_N = 17$ K, held for a few minutes, and then cooled to the target temperature with no applied magnetic field. After stabilizing the temperature, the magnetic field was first increased to 9 T, then decreased to -9 T and swept to 0 T. At 8 K an irreversible behavior is clearly seen; during the first field sweep the specific heat below 4.5 T is higher than for the second sweep from $+9$ to -9 T, indicating the formation of a field-induced metastable phase, which is also observed in transport measurements.

To explore the observed transitions further, we have studied the thermal and magnetic-field dependencies of specific heat (C_p). Previously the $C_p(T,H)$ has been successfully used to construct the phase diagram for $GdNiC_2$ [49]. Figure 12 shows a specific-heat map (a) and the heat capacity of the polycrystalline $CeNiC_2$ (b) plotted as a function of temperature, under various magnetic fields. In the results we can observe a few anomalies. The largest one is seen at about 19 K and is almost unaffected by the applied magnetic fields up to 9 T. The second anomaly is less pronounced, and the

temperature of its occurrence varies with the applied magnetic field from 11 K in 0 T to 9.5 K in 9 T. The existence of these features is in agreement with magnetization and transport results. Another anomaly, previously reported by Motoya *et al.* [46], seen at 2 K, is magnetic-field dependent. A minor jump around 30 K is likely connected with the CeC_2 impurity phase [44], as suggested from magnetic susceptibility data.

The broad hump seen in $PrNiC_2$ [Figs. 12(c) and 12(d)] is a Schottky anomaly originating from multiple energy levels of the Pr^{3+} ion subject to the CEF splitting. Due to the complicated energy level structure the specific-heat data could not be reliably fitted in order to extract the level splitting energies. The anomaly is slightly shifted towards higher temperature by applied magnetic field as seen in Fig. 12(c) and 12(d), which is caused by the Zeeman effect, as seen in many *f*-electron systems (see, e.g., [78–80]). No clear anomaly is seen around T^*, corresponding both to the drop in the Hall resistivity and the upturn of magnetic susceptibility. This may suggest that the alleged transition involves predominantly the change of electronic structure with little effect on crystal and spin order, which should result in the appearance of an anomaly in specific heat. Note that in the $Pb_2Sr_2PrCu_3O_8$ compound mentioned before the specific-heat anomaly at the transition temperature is weak [81]. If such weak anomaly would arise in $PrNiC_2$ at the T^*, it could be hard to observe on top of the large Schottky hump.

The results of the specific-heat measurements for $NdNiC_2$ are shown in Figs. 12(e) and 12(f). For this compound the specific heat shows a λ-like anomaly at T_N, which is weakly affected by the applied magnetic field up to about 3.0–3.5 T, above which a metamagnetic transition occurs. Above 7 T we can observe the third anomaly, which is probably related to the occurrence of the transitional phase between AFM and FM.

The magnetic-field dependence of the specific heat of $NdNiC_2$ measured at 12 K, 10 K, and 8 K is presented in Fig. 13. At 8 K the C_p vs H shows an irreversible behavior, as seen in Fig. 13(c). The observation of the irreversibility in both specific-heat and electrical-resistivity measurements confirms the presence of a magnetic-field-induced metastable state, not reported in previous studies. Interestingly, the same transition does not result in the appearance of hysteresis in magnetization, as seen in the inset of Fig. 3. This could be explained by the insufficient resolution of magnetization measurements performed with the ACMS option. However, it is also possible that the field-induced transition involves a change of electronic and crystal structures without a significant change in magnetic order.

IV. CONCLUSIONS

In order to explore the interaction between charge density waves and magnetism in the $RNiC_2$ family, we have compared the physical properties of three isostructural compounds: $NdNiC_2$, showing both the Peierls instability; $PrNiC_2$ with the CDW and a magnetic anomaly; and $CeNiC_2$, showing antiferromagnetic ordering and the absence of the CDW transition. The weak magnetoresistance in $CeNiC_2$ is found to originate from the spin fluctuations accompanying the magnetic transition. Neither transport nor Hall effect measurements reveal any signatures of the Peierls instability. Study of the magnetoresistance and the galvanomagnetic properties of $NdNiC_2$ confirms the partial suppression of charge density waves by magnetic ordering and a further destruction of the Peierls instability at the crossover from the antiferromagnetic to ferromagnetic order. We have also found that this magnetic transformation drives a metastable lattice transformation that can be observed via the magnetoresistance and the specific-heat measurements. The interplay between magnetism and charge density waves in $PrNiC_2$ shows more complex character. Although the magnetoresistance data suggest that the application of magnetic field partially suppresses CDW by Zeeman splitting of the electronic bands, the expansion of the nested region of the Fermi surface at $T^* \approx 8$ K can be observed by a significant downturn of the Hall resistivity, strong enough to overcome the positive Hall signal originating from the anomalous component. This effect seems to be related to the magnetic anomaly [43] observed at the same temperature; however, the underlying mechanism remains unclear. Tentatively, the interaction between the CDW and magnetic properties of this compound can be described either by the lattice transformation due to the magnetic anomaly, and by the modification of the magnetic ordering via the RKKY interactions influenced by change of the electronic concentration. Further analysis of this effect can be realized by high-resolution diffraction experiments on a single crystal.

ACKNOWLEDGMENTS

Authors gratefully acknowledge financial support from National Science Centre (Poland), Grant No. UMO-2015/19/B/ST3/03127. We also thank E. Carnicom, K. Rogacki, Z. Sobczak, K. Górnicka, and H. Marciniak for useful advice and fruitful discussions.

[1] J. Chang, E. Blackburn, A. T. Holmes, N. B. Christensen, J. Larsen, J. Mesot, R. Liang, D. A. Bonn, W. N. Hardy, A. Watenphul, M. v. Zimmermann, E. M. Forgan, and S. M. Hayden, Nat. Phys. **8**, 871 (2012).

[2] E. H. da Silva Neto, P. Aynajian, A. Frano, R. Comin, E. Schierle, E. Weschke, A. Gyenis, J. Wen, J. Schneeloch, Z. Xu, S. Ono, G. Gu, M. Le Tacon, and A. Yazdani, Science **343**, 393 (2014).

[3] J. Chang, E. Blackburn, O. Ivashko, A. T. Holmes, N. B. Christensen, M. Hücker, R. Liang, D. A. Bonn, W. N. Hardy, U. Rütt, M. v. Zimmermann, E. M. Forgan, and S. M. Hayden, Nat. Commun. **7**, 11494 (2016).

[4] E. Fawcett, Rev. Mod. Phys. **60**, 209 (1988).

[5] V. L. R. Jacques, C. Laulhé, N. Moisan, S. Ravy, and D. Le Bolloc'h, Phys. Rev. Lett. **117**, 156401 (2016).

[6] C. Y. Young and J. B. Sokoloff, J. Phys. F **4**, 1304 (1974).

[7] C. A. Balseiro, P. Schlottmann, and F. Yndurain, Phys. Rev. B **21**, 5267 (1980).

[8] T. Tiedje, J. F. Carolan, A. J. Berlinsky, and L. Weiler, Can. J. Phys. **53**, 1593 (1975).

[9] J. Brooks, D. Graf, E. Choi, M. Almeida, J. Dias, R. Henriques, and M. Matos, Curr. Appl. Phys. **6**, 913 (2006).

[10] J.-F. Wang, M. Yang, L. Li, M. Sasaki, A. Ohnishi, M. Kitaura, K.-S. Kim, and H.-J. Kim, Phys. Rev. B **89**, 035137 (2014).

[11] D. Andres, M. V. Kartsovnik, W. Biberacher, K. Neumaier, I. Sheikin, H. Müller, and N. D. Kushch, Low Temp. Phys. **37**, 762 (2011).

[12] D. Zanchi, A. Bjeliš, and G. Montambaux, Phys. Rev. B **53**, 1240 (1996).

[13] D. Graf, E. S. Choi, J. S. Brooks, R. T. Henriques, M. Almeida, and M. Matos, Phys. Rev. Lett. **93**, 076406 (2004).

[14] L. E. Winter, J. S. Brooks, P. Schlottmann, M. Almeida, S. Benjamin, and C. Bourbonnais, Europhys. Lett. **103**, 37008 (2013).

[15] K. Murata, Y. Fukumoto, K. Yokogawa, W. Kang, R. Takaoka, R. Tada, H. Hirayama, J. S. Brooks, D. Graf, H. Yoshino, T. Sasaki, and R. Kato, Phys. B (Amsterdam, Neth.) **460**, 241 (2015).

[16] P. C. Lalngilneia, A. Thamizhavel, S. Ramakrishnan, and D. Pal, J. Phys.: Conf. Ser. **592**, 012094 (2015).

[17] S. van Smaalen, M. Shaz, L. Palatinus, P. Daniels, F. Galli, G. J. Nieuwenhuys, and J. A. Mydosh, Phys. Rev. B **69**, 014103 (2004).

[18] F. Galli, S. Ramakrishnan, T. Taniguchi, G. J. Nieuwenhuys, J. A. Mydosh, S. Geupel, J. Lüdecke, and S. van Smaalen, Phys. Rev. Lett. **85**, 158 (2000).

[19] F. Galli, R. Feyerherm, R. W. A. Hendrikx, E. Dudzik, G. J. Nieuwenhuys, S. Ramakrishnan, S. D. Brown, S. van Smaalen, and J. A. Mydosh, J. Phys.: Condens. Matter **14**, 5067 (2002).

[20] Z. Hossain, M. Schmidt, W. Schnelle, H. S. Jeevan, C. Geibel, S. Ramakrishnan, J. A. Mydosh, and Y. Grin, Phys. Rev. B **71**, 060406 (2005).

[21] M. Leroux, P. Rodière, and C. Opagiste, J. Supercond. Novel Magn. **26**, 1669 (2013).

[22] Y. Singh, D. Pal, and S. Ramakrishnan, Phys. Rev. B **70**, 064403 (2004).

[23] N. S. Sangeetha, A. Thamizhavel, C. V. Tomy, S. Basu, A. M. Awasthi, S. Ramakrishnan, and D. Pal, Phys. Rev. B **86**, 024524 (2012).

[24] Y. K. Kuo, K. M. Sivakumar, T. H. Su, and C. S. Lue, Phys. Rev. B **74**, 045115 (2006).

[25] J. N. Kim, C. Lee, and J.-H. Shim, New J. Phys. **15**, 123018 (2013).

[26] G. Prathiba, I. Kim, S. Shin, J. Strychalska, T. Klimczuk, and T. Park, Sci. Rep. **6**, 26530 (2016).

[27] M. Murase, A. Tobo, H. Onodera, Y. Hirano, T. Hosaka, S. Shimomura, and N. Wakabayashi, J. Phys. Soc. Jpn. **73**, 2790 (2004).

[28] N. Yamamoto, R. Kondo, H. Maeda, and Y. Nogami, J. Phys. Soc. Jpn. **82**, 123701 (2013).

[29] J. Laverock, T. D. Haynes, C. Utfeld, and S. B. Dugdale, Phys. Rev. B **80**, 125111 (2009).

[30] D. Ahmad, B. H. Min, G. I. Min, S.-I. Kimura, J. Seo, and Y. S. Kwon, Phys. Status Solidi (B) **252**, 2662 (2015).

[31] S. Shimomura, C. Hayashi, N. Hanasaki, K. Ohnuma, Y. Kobayashi, H. Nakao, M. Mizumaki, and H. Onodera, Phys. Rev. B **93**, 165108 (2016).

[32] A. Wölfel, L. Li, S. Shimomura, H. Onodera, and S. van Smaalen, Phys. Rev. B **82**, 054120 (2010).

[33] W. Lee, H. Zeng, Y. Yao, and Y. Chen, Phys. C (Amsterdam, Neth.) **266**, 138 (1996).

[34] V. K. Pecharsky, L. L. Miller, and K. A. Gschneidner, Phys. Rev. B **58**, 497 (1998).

[35] B. Wiendlocha, R. Szczęśniak, A. P. Durajski, and M. Muras, Phys. Rev. B **94**, 134517 (2016).

[36] W. Schäfer, W. Kockelmann, G. Will, J. Yakinthos, and P. Kotsanidis, J. Alloys Compd. **250**, 565 (1997).

[37] P. Kotsanidis, J. Yakinthos, and E. Gamari-Seale, J. Less-Common Met. **152**, 287 (1989).

[38] A. Bhattacharyya, D. T. Adroja, A. M. Strydom, A. D. Hillier, J. W. Taylor, A. Thamizhavel, S. K. Dhar, W. A. Kockelmann, and B. D. Rainford, Phys. Rev. B **90**, 054405 (2014).

[39] J. Yakinthos, P. Kotsanidis, W. Schäfer, and G. Will, J. Magn. Magn. Mater. **89**, 299 (1990).

[40] N. Hanasaki, K. Mikami, S. Torigoe, Y. Nogami, S. Shimomura, M. Kosaka, and H. Onodera, J. Phys.: Conf. Ser. **320**, 012072 (2011).

[41] N. Uchida, H. Onodera, M. Ohashi, Y. Yamaguchi, N. Sato, and S. Funahashi, J. Magn. Magn. Mater. **145**, L16 (1995).

[42] S. Matsuo, H. Onodera, M. Kosaka, H. Kobayashi, M. Ohashi, H. Yamauchi, and Y. Yamaguchi, J. Magn. Magn. Mater. **161**, 255 (1996).

[43] H. Onodera, Y. Koshikawa, M. Kosaka, M. Ohashi, H. Yamauchi, and Y. Yamaguchi, J. Magn. Magn. Mater. **182**, 161 (1998).

[44] T. Sakai, G.-y. Adachi, and J. Shiokawa, Mater. Res. Bull. **15**, 1001 (1980).

[45] J. Rodríguez-Carvajal, Phys. B (Amsterdam, Neth.) **192**, 55 (1993).

[46] K. Motoya, K. Nakaguchi, N. Kayama, K. Inari, J. Akimitsu, K. Izawa, and T. Fujita, J. Phys. Soc. Jpn. **66**, 1124 (1997).

[47] W. Schäfer, G. Will, J. Yakinthos, and P. Kotsanidis, J. Alloys Compd. **180**, 251 (1992).

[48] J. Jensen and A. R. Mackintosh, *Rare Earth Magnetism: Structures and Excitations* (Clarendon Press, Oxford, UK, 1991).

[49] K. K. Kolincio, K. Górnicka, M. J. Winiarski, J. Strychalska-Nowak, and T. Klimczuk, Phys. Rev. B **94**, 195149 (2016).

[50] W. T. Hsieh, W.-H. Li, K. C. Lee, J. W. Lynn, J. H. Shieh, and H. C. Ku, J. Appl. Phys. **76**, 7124 (1994).

[51] S. Akamaru, Y. Isikawa, J. Sakurai, K. Maezawa, and H. Harima, J. Phys. Soc. Jpn. **70**, 2049 (2001).

[52] J. L. Snyman and A. M. Strydom, J. Appl. Phys. **113**, 17E135 (2013).

[53] A. Gil, A. Szytuła, Z. Tomkowicz, K. Wojciechowski, and A. Zygmunt, J. Magn. Magn. Mater. **129**, 271 (1994).

[54] K. Kolincio, O. Pérez, S. Hébert, P. Fertey, and A. Pautrat, Phys. Rev. B **93**, 235126 (2016).

[55] H. Lei, K. Wang, and C. Petrovic, J. Phys.: Condens. Matter **29**, 075602 (2017).

[56] K. Usami, J. Phys. Soc. Jpn. **45**, 466 (1978).

[57] C. Mazumdar, A. K. Nigam, R. Nagarajan, L. C. Gupta, G. Chandra, B. D. Padalia, C. Godart, and R. Vijayaraghaven, J. Appl. Phys. **81**, 5781 (1997).

[58] H. Yamada and S. Takada, Prog. Theor. Phys. **48**, 1828 (1972).

[59] S. Shimomura, C. Hayashi, G. Asaka, N. Wakabayashi, M. Mizumaki, and H. Onodera, Phys. Rev. Lett. **102**, 076404 (2009).

[60] N. Hanasaki, Y. Nogami, M. Kakinuma, S. Shimomura, M. Kosaka, and H. Onodera, Phys. Rev. B **85**, 092402 (2012).
[61] W. Dieterich and P. Fulde, Z. Phys. A **265**, 239 (1973).
[62] X. Xu, A. F. Bangura, J. G. Analytis, J. D. Fletcher, M. M. J. French, N. Shannon, N. E. Hussey, J. He, S. Zhang, D. Mandrus, and R. Jin, Phys. Rev. Lett. **102**, 206602 (2009).
[63] D. Graf, J. S. Brooks, E. S. Choi, S. Uji, J. C. Dias, M. Almeida, and M. Matos, Phys. Rev. B **69**, 125113 (2004).
[64] M. Matos, G. Bonfait, R. T. Henriques, and M. Almeida, Phys. Rev. B **54**, 15307 (1996).
[65] G. Bonfait, M. J. Matos, R. T. Henriques, and M. Almeida, Phys. B (Amsterdam, Neth.) **211**, 297 (1995).
[66] G. Bonfait, E. B. Lopes, M. J. Matos, R. T. Henriques, and M. Almeida, Solid State Commun. **80**, 391 (1991).
[67] D. Graf, E. Choi, J. Brooks, J. Dias, R. Henriques, M. Almeida, M. Matos, and D. Rickel, Synth. Met. **153**, 361 (2005).
[68] K. Monchi, M. Poirier, C. Bourbonnais, M. Matos, and R. Henriques, Synth. Met. **103**, 2228 (1999).
[69] E. Wang, M. Greenblatt, I. E.-I. Rachidi, E. Canadell, M.-H. Whangbo, and S. Vadlamannati, Phys. Rev. B **39**, 12969 (1989).
[70] C. Schlenker, J. Dumas, C. Escribe-filippini, H. Guyot, J. Marcus, and G. Fourcaudot, Philos. Mag. B **52**, 643 (1985).
[71] J. H. Kim, J.-S. Rhyee, and Y. S. Kwon, Phys. Rev. B **86**, 235101 (2012).
[72] L. Berger and G. Bergmann, in *The Hall Effect and Its Applications*, edited by C. L. Chien and C. R. Westgate (Springer US, Boston, 1980), pp. 55–76.
[73] J. S. Higgins, S. R. Shinde, S. B. Ogale, T. Venkatesan, and R. L. Greene, Phys. Rev. B **69**, 073201 (2004).
[74] Q. Xu, L. Hartmann, H. Schmidt, H. Hochmuth, M. Lorenz, R. Schmidt-Grund, C. Sturm, D. Spemann, and M. Grundmann, Phys. Rev. B **73**, 205342 (2006).
[75] A. Oiwa, A. Endo, S. Katsumoto, Y. Iye, H. Ohno, and H. Munekata, Phys. Rev. B **59**, 5826 (1999).
[76] Y. Shiomi, Y. Onose, and Y. Tokura, Phys. Rev. B **79**, 100404 (2009).
[77] K. Rogacki (private communication).
[78] M. J. Winiarski and T. Klimczuk, J. Solid State Chem. **245**, 10 (2017).
[79] M. Tachibana, Y. Kohama, T. Atake, and E. Takayama-Muromachi, J. Appl. Phys. **101**, 09D502 (2007).
[80] T. Mori, T. Takimoto, A. Leithe-Jasper, R. Cardoso-Gil, W. Schnelle, G. Auffermann, H. Rosner, and Y. Grin, Phys. Rev. B **79**, 104418 (2009).
[81] S. Y. Wu, Y. C. Chang, K. C. Lee, and W.-H. Li, J. Appl. Phys. **83**, 7318 (1998).